Interactions in 1-Ethyl-3-Methyl Imidazolium Tetracyanoborate Ion Pair: A Density Functional Study

James X. Mao,[†] Anita Lee,[‡] Hunaid B. Nulwala,[¶] David R. Luebke,[¶] and Krishnan Damodaran[*,†]

Department of Chemistry, University of Pittsburgh, Pittsburgh, Pennsylvania 15260, Department of Chemistry, Carnegie Mellon University, Pittsburgh, Pennsylvania 15213, and National Energy Technology Laboratory, P.O. Box 10940, Pittsburgh, Pennsylvania 15236

E-mail: damodak@pitt.edu

Phone: 412-624-8403. Fax: 412-624-8611

[*]To whom correspondence should be addressed

[†]Department of Chemistry, University of Pittsburgh, Pittsburgh, Pennsylvania 15260

[‡]Department of Chemistry, Carnegie Mellon University, Pittsburgh, Pennsylvania 15213

[¶]National Energy Technology Laboratory, P.O. Box 10940, Pittsburgh, Pennsylvania 15236

Abstract

Density Functional Theory is used to investigate a weakly coordinating room-temperature ionic liquid, 1-ethyl-3-methyl imidazolium tetracyanoborate ($[Emim]^+[TCB]^-$). Four locally stable conformers of the ion pair were located. Atoms-in-molecules (AIM) and electron density analysis indicated the existence of several hydrogen bonds. Further investigation through the Natural Bond Orbital (NBO) and Natural Energy Decomposition Analysis (NEDA) calculations provided insight into the origin of interactions in the $[Emim]^+[TCB]^-$ ion pair. Strength of molecular interactions in the ionic liquid was correlated with frequency shifts of the characteristic vibrations of the ion pair. Harmonic vibrations of the ion pair were also compared with the experimental Raman and Infrared spectra. Vibrational frequencies were assigned by visualizing displacements of atoms around their equilibrium positions and through Potential Energy Distribution (PED) analysis.

Introduction

Room-temperature ionic liquids (RTILs) are salts which have low melting points (melting point below 100 °C). They normally possess a bulky and asymmetric organic cation which inhibits an ordered crystalline structure to form. Many of their unique properties, such as very low vapor pressure, nonflammability, electrochemical and thermal stability, have gained them promising applications in a wide variety of fields. They have been used as environmentally friendly solvents for reactions, electrolytes for high efficiency electrochemical devices, entrainers for gas or liquid separation processes, and lubricant in tribological applications.

BF_4^- has been a well-known and widely used RTIL anion. However, at high temperature BF_4^- is hydrolytically unstable and produces HF following the reaction with water. By replacing all fluorine atoms of BF_4^- ion with cyano groups, the new tetracyanoborate ($[TCB]^-$) based RTILs are hydrolytically stable and exhibit many promising applications. These RTILs can be used as solvents to accelerate the free radical polymerization of unsaturated monomers: their high polarity increase the propagation rate and their viscosity decrease the termination rate.[1] They can be

used as electrolytes due to their high chemical and thermal stability in mesoscopic dye-sensitized solar cells, a promising low-cost device for the sustainable energy supply in the future.[2,3] Indeed, RTIL 1-ethyl-3-methyl imidazolium tetracyanoborate ($[Emim]^+[TCB]^-$) shows higher oxidation potential compared to other boron-containing anions.[4] They are also very promising in separation and extraction processes. In the separation of aromatic from aliphatic hydrocarbons, a process that plays a key role in chemical industry, $[Emim]^+[TCB]^-$ exhibits higher selectivity and capacity at infinite dilution than the generally used organic solvents and many other RTILs containing the same $[Emim]^+$ cation.[5–7] The use of supported liquid membranes for gas separation is a promising technique for removing greenhouse gas from power plant emissions or natural gas streams, and $[Emim]^+[TCB]^-$ based membranes were shown to yield the highest known permeance with excellent CO_2/N_2 separation selectivity. For example, it was found the CO_2 solubility in $[Emim]^+[TCB]^-$ is about 30% higher than another popular RTIL $[Emim]^+[TF2N]^-$.[8]

Understanding RTILs' interesting physicochemical properties, especially the role of weak interaction between cation and anion, is the key to many of their efficient applications. Ionic liquids with weak cation-anion interactions are less prone to the formation of cation-anion ion pairs. These type of RTILs usually posses higher conductivities, which increases their importance for development of new energy-related devices.[9] It was also pointed out that the weak interaction between cation and anion could be the dominant factor responsible for high CO_2 solubility.[10] Weak cation-anion interaction allows easy expansion of cavities of the ionic liquid structure, so more CO_2 molecules can occupy free volume. The importance of preparing weakly coordinating RTILs has been realized and more new ionic liquids were proposed and synthesized to achieve weaker cation-anion interaction and better CO_2 capture. To shed more light on the mechanism behind weakly coordinating RTILs' unique physiochemical properties, the molecular interactions between cation and anion of $[Emim]^+[TCB]^-$, a typical weakly coordinating RTIL, were studied and reported by density functional theory in this work.

Quantum Mechanical Method

Calculations were performed at Density Function Theory (DFT) level with the hybrid functional B3LYP, which incorporates Becke's three-parameter exchange functional[11] and the Lee, Yang, and Parr correlation functional[12] using the Gaussian 09 program.[13] The 6-31+G(d, p) basis sets[14] implemented in the Gaussian program were used. The geometries of ion pairs were fully optimized at the B3LYP/6-31+G(d, p) level, and the basis set superposition error (BSSE)[15] was corrected for all interaction calculations using the counterpoise method.[16,17] Zero-point energies (ZPE) were also corrected for all optimized structures, and frequencies were calculated to ensure that no imaginary components existed. Natural bond orbital (NBO)[18] and atoms in molecules (AIM)[19,20] analyses were carried out by programs implemented in the Gaussian 09 and Firefly QC package[21] to study the interactions between ion pairs. Vibrational frequencies were assigned by visualizing displacements of atoms around their equilibrium positions and through Potential Energy Distribution (PED) analysis.

Experimental

Chemical

1-Ethyl-3-methylimidazolium tetracyanoborate (CAS# 742099-80-5) was purchased from EMD chemicals and used without further purification.

Infrared and Raman Spectroscopy

The IR spectrum was collected from 400 to 4000 cm^{-1} on an attenuated total reflection (ATR) module with a Nicolet Model 360 FTIR at 2 cm^{-1} nominal resolution. The number of reflections at the diamond crystal surface is "1", and the penetration depth of the system is approximately one-fifth of the wavelength. For the measurement, a droplet of the IL was placed on the ATR crystal under dry nitrogen flow.

Results and Discussion

Geometric Analysis

The ethyl group bound to the imidazolium ring in $[Emim]^+$ ion is able to rotate to yield different conformers. Both computational and experimental works[22,23] showed there exist two stable $[Emim]^+$ structures, a planar C_s structure and a non-planar C_1 structure (Figure 1). The C_1 structure is slightly favored by 2.3 kJ/mol. Umebayashi *et al.* showed the presence of both conformers in RTIL $[Emim]^+[BF_4]^-$ at a population of 3:2.[23] It is certainly expected that both of the conformers exist in RTIL $[Emim]^+[TCB]^-$ as well for their small energy difference. Therefore, for geometric optimizations $[TCB]^-$ ion was placed around both planar and non-planar conformers of $[Emim]^+$ ion in various positions.

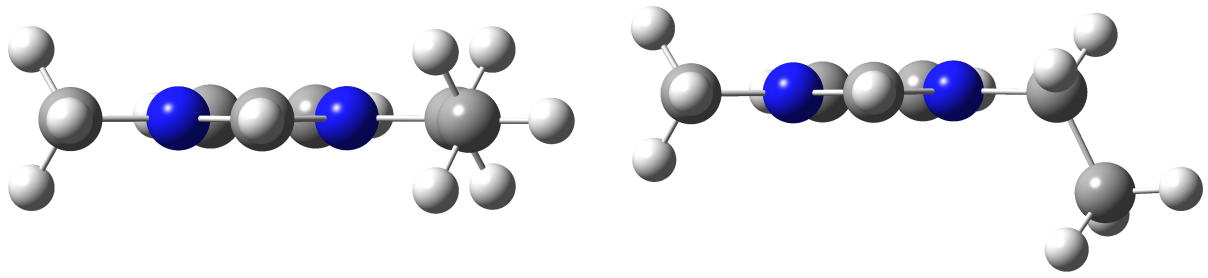

(a) (b)

Figure 1: $[Emim]^+$ cation conformers optimized at the B3LYP/6-31+G** level. (a): C_s planar structre. (b): C_1 non-planar structure. The non-planar structure is slightly more stable than planar structure by 2.3 kJ/mol.

Four stable structures of $[Emim]^+[TCB]^-$ ion pair were located during optimization calculations, and they are shown in Figure 2. These stable geometries were confirmed to be local minima on the potential energy surface through vibrational frequency analysis (no imaginary components). Their energy (E), lowest vibrational frequencies, along with zero-point vibrational energy corrections, are listed in Table 1.

Among the four stable structures (shown in Figure 2), the only one structure in which $[Emim]^+$ takes the C_s planar conformer is structure (d) and it is least stable. In the most stable structure (a), the anion $[TCB]^-$ lies below the non-planar cation $[Emim]^+$. By avoiding the ethyl group from below, the anion can move closer to the imidazolium ring to maximize hydrogen bonding interactions between cation and anion, thereby lowering the total energy. In structure (b) and (c), $[TCB]^-$ ion lies above the imidazolium ring of cation $[Emim]^+$.

Table 1: Energies [a], lowest vibrational frequencies, energies with ZPE corrections, interaction energies [b], and Natural Energy Decomposition Analysis (NEDA) for different $[Emim]^+[TCB]^-$ conformations. Energy in unit of kJ/mol.

Conformation	E	Lowest Vibrational Frequencies /cm^{-1}	E+ZPE	E(int)	Natural Energy Decomposition		
					Charge Transfer	Electrical	Core
a	0	27	0	286.6	67.5	360.7	-141.6
b	4.5	20	4.9	284.9	64.4	349.5	-128.9
c	6.1	22	5.9	280.6	62.1	356.7	-138.3
d	1.2	22	1.8	279.7	100.3	353.3	-173.9
$[Emim]^+[BF_4]^-$				352.6	104.1	435.0	-186.5

[a] Relative energies. [b] Where BSSE correction is considered.

Interaction Energy and AIM Analysis

Interaction energies were calculated as the difference between the energies of the cation-anion pair and the sum of the energies of the sole cation and anion species,

$$E(\text{int}) = E([Emim]^+[TCB]^-) - E([Emim]^+) - E([TCB]^-)$$

The counterpoise approach[16] was applied to correct basis-set superposition error (BSSE)[15] and results are shown in Table 1. Comparing to the reported interaction energies for $[Emim]^+[BF_4]^-$ ion pairs which are around 364 kJ/mol,[24] interaction energies for $[Emim]^+[TCB]^-$ ion pairs (around 280 kJ/mol) are much weaker. These weaker interaction energies possibly enable more free volume in $[Emim]^+[TCB]^-$, resulting in an enhanced CO_2 capture ability.[8]

AIM analysis[25] was carried out to identify the interactions between $[Emim]^+$ cation and $[TCB]^-$ anion. In AIM analysis, critical points are classified by the number of eigenvalues and positive

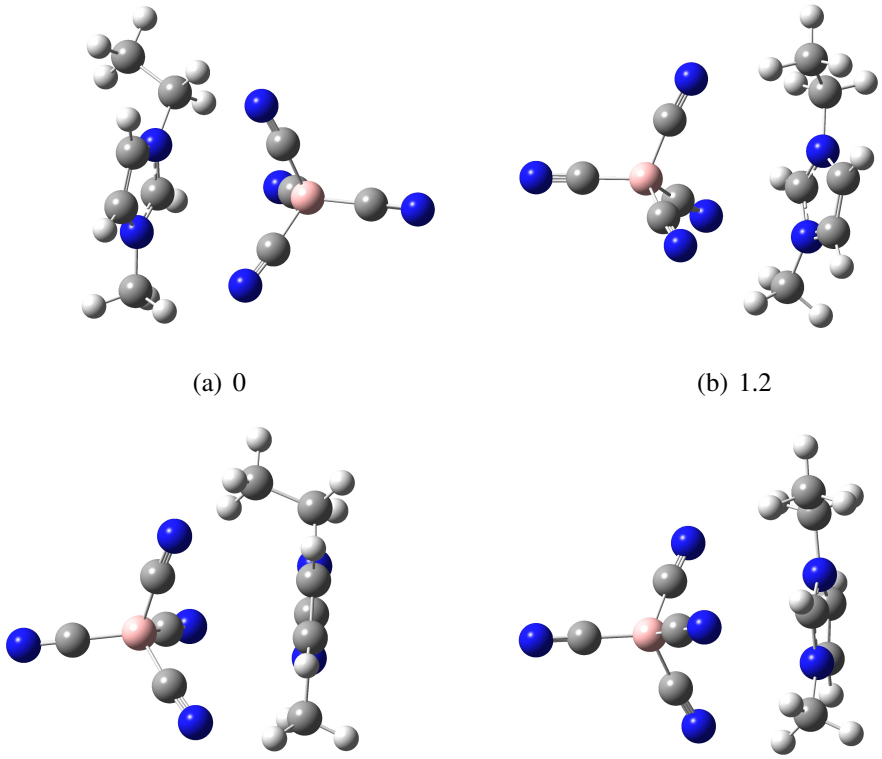

(a) 0 (b) 1.2

(c) 4.5 (d) 6.1

Figure 2: Optimized stable $[Emim]^+[TCB]^-$ ion pair structures. Relative energy in kJ/mol.

eigenvalues of the Hessian matrix of molecular electron density. A bond critical point is a critical point with three non-zero eigenvalues and exactly one of them is negative. An electron density at the bond critical point in the range of 0.002-0.035 au has been proposed as a criterion to confirm and characterize existence of a hydrogen bond.[19,20] For the most stable $[Emim]^+[TCB]^-$ structure (a), four inter-ionic bond critical points were identified by AIM analysis (Figure 3). Electron densities at the four located bond critical points were calculated and shown in Figure 3. They are all in range of 0.005-0.011 au, which confirm the existence of hydrogen bondings.

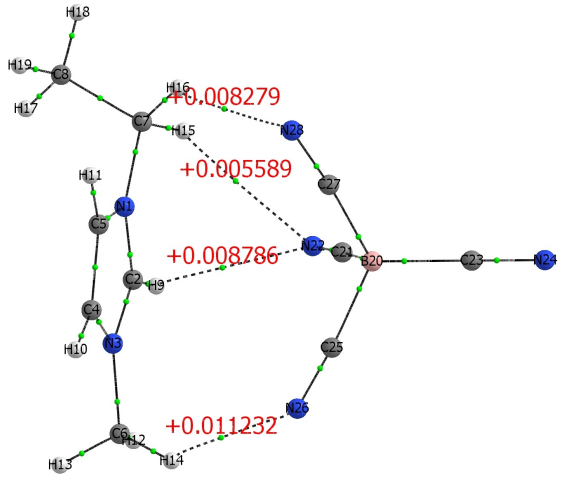

Figure 3: $[Emim]^+ \cdots [TCB]^-$ inter-ionic hydrogen bonding for most stable conformation. Critical bond points are marked by green points, and electron densities (in atomic units) at inter-ionic critical bond points are shown aside.

Inter-ionic interactions induce the electron density reorganization between cations and anions, and the reorganization can be presented by plotting the difference in electron density ($\Delta\rho = \rho_{\text{ion pair}} - \rho_{\text{cation}} - \rho_{\text{anion}}$) map. The difference electron density map for the most stable $[Emim]^+$ $[TCB]^-$ conformation was calculated and shown in Figure 4. The purple region shows where electron density is enhanced, and the turquoise region is where electron density is depleted. Note that bonds in the region where electron density is enhanced are strengthened, and bonds in the region where electron density is depleted are weakened. It is important to note that all four inter-ionic critical bond points are situated in the purple region where electron density increases.

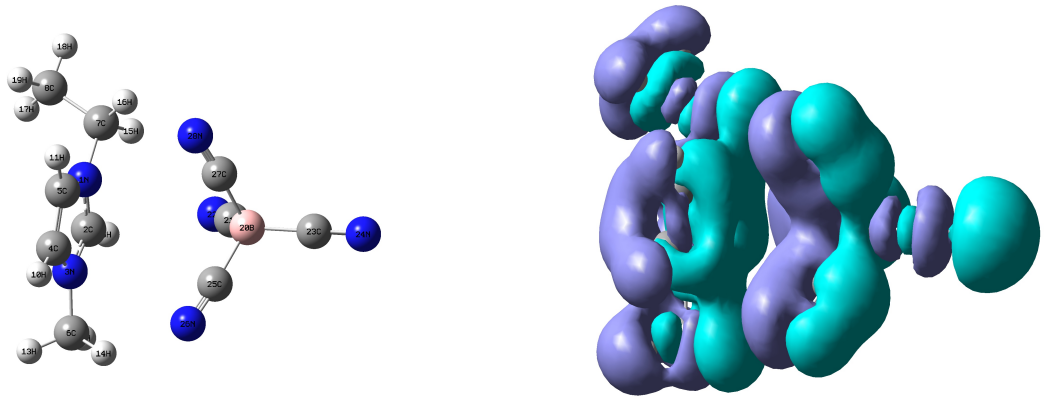

(a) (b)

Figure 4: (a): Atom numbering scheme. (b) Corresponding difference electron density ($\Delta\rho = \rho_{\text{ion pair}} - \rho_{\text{cation}} - \rho_{\text{anion}}$) map of most stable $[\text{Emim}]^+[\text{TCB}]^-$ ion pair conformation. Purple region is where $\Delta\rho > 0$ and turquoise region is where $\Delta\rho < 0$.

Natural Energy Decomposition Analysis

Natural Energy Decomposition Analysis (NEDA)[18,26,27] identifies interactions into three components: electrical component, core component, and charge transfer component. Electrical component represents the classical-like Coulombic interactions, core component represents repulsions at the equilibrium position which is inside van der Waals contact, and charge transfer represents delocalization interactions between subunits:

$$\Delta E = E(\text{Electrical}) + E(\text{Core}) + E(\text{Charge Transfer})$$

Charge transfer interactions can be calculated using NBO analysis[28,29] by deleting all inter-ionic delocalization of electron density while retaining all intra-ionic delocalizations. The NEDA results are shown in Table 1. It was not surprising that the electrical components are the largest individual contributors to the total interactions between cation and anion for a RTIL. Also, it is shown clearly that the charge transfer is another very important component. One thing is interesting to notice is that although the charge transfer component changes a lot when $[\text{Emim}]^+$ takes its C_s planar structure in structure (d), the electrical component and the total interaction do not change a lot

from other structures where $[Emim]^+$ takes its C_1 non-planar structure.

NEDA was also carried out for an optimized $[Emim]^+[BF_4]^-$ ion pair and the results are shown in Table 1. While comparing with $[Emim]^+[TCB]^-$ interactions, it seems the decrease in interaction energies from $[Emim]^+[BF_4]^-$ to $[Emim]^+[TCB]^-$ are mainly due to the electrical component. This is reasonable since the distance between cation and anion increases from $[Emim]^+[BF_4]^-$ ion pairs to $[Emim]^+[TCB]^-$ ion pairs.

Infrared and Raman Spectra Analysis

Harmonic vibrations for most stable $[Emim]^+[TCB]^-$ ion pair were calculated at B3LYP/6-31+G** level and scaled by a factor of 0.958 to compared with experimental Raman and infrared spectra (Figure 5). The correlation diagram between calculated frequencies and experimental frequencies shows a correlation coefficient 0.9998 (Figure 6). The spectra were then compared to other documented RTIL spectra to obtain quantitative understanding of the inter-ionic interactions.

The most strong peak in the Raman spectrum is the anion CN stretching mode at 2225 cm^{-1}. It has been shown that the wavenumber of this mode is a good indicator for the inter-ionic interaction: strong interaction will move the mode to high wavenumber.[30] Compared to the documented positions of this peak in other RTILs with anion $[TCB]^-$ (Table 2), the interaction between $[Emim]^+$ and $[TCB]^-$ is weaker than the ones with smaller cation and almost the same as $[Bmim]^+[TCB]^-$.

Table 2: CN stretching mode positions for different $[B(CN)_4]^-$ ILs. Data except $[Emim]^+[B(CN)_4]^-$ are from Reference.[30]

Compound	ν(CN) /cm^{-1}	
	Raman	IR
$Li^+[TCB]^-$	2263	2262
$Na^+[TCB]^-$	2252	2252
$K^+[TCB]^-$	2233	2234
$NH_4^+[TCB]^-$	2233	2234
$[Bmim]^+[TCB]^-$	2224	2223
$[Emim]^+[TCB]^-$	2225	2225

It now seems that the origin of the ν(CH) vibrations profile (modes higher than 2500 cm^{-1})

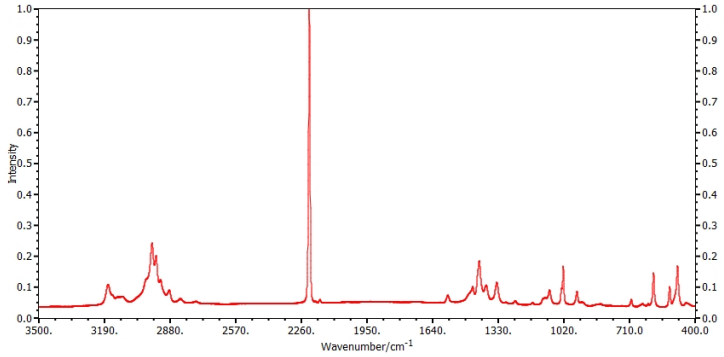

(a) Raman Spectrum

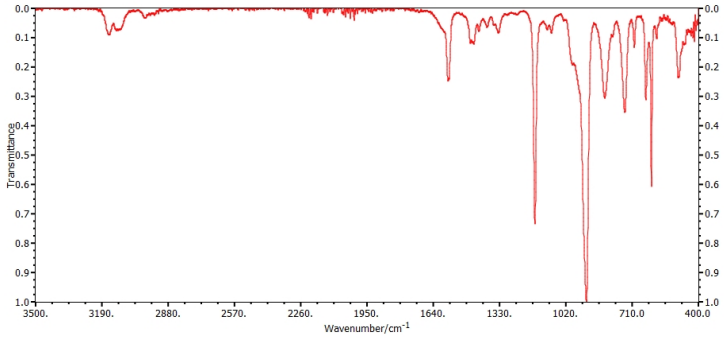

(b) Infrared Spectrum

Figure 5: Raman and IR spectra of $[Emim]^+[TCB]^-$. Range from 400 cm^{-1} to 3500 cm^{-1}.

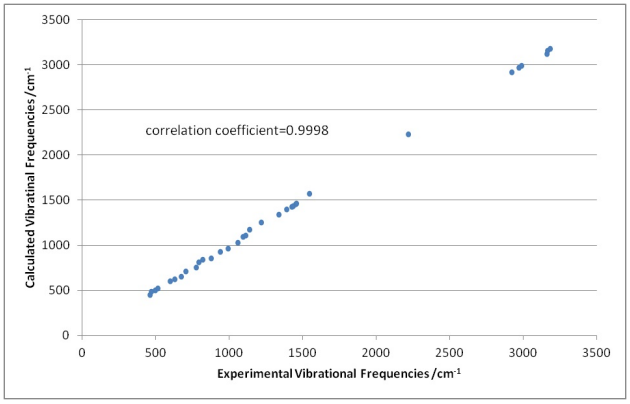

Figure 6: Correlation diagram for the vibrational spectrum of $[Emim]^+[TCB]^-$. Scaling factor is 0.958 with a resulted correlation coefficient 0.9998.

is very complicated, thus not a good indicator for the inter-ionic interaction.[31] Instead, the γ(CH) mode in the range of 800-850 cm^{-1} has been suggested to be used as direct spectroscopic probes of the cation-anion interactions since it changes noticeably in different ILs.[32] Increasing interactions are expected to produce blue shift of this mode. A red shift of 11 cm^{-1}, from 850 cm^{-1} in $[Emim]^+[BF_4]^-$ to 839 cm^{-1} in $[Emim]^+[TCB]^-$, clearly confirms weakening interactions.

Another interesting observation from the experimental Raman spectrum is the co-existence of planar and non-planar conformers of $[Emim]^+$ ion in $[Emim]^+[TCB]^-$ RTIL. The co-existence of both conformers in many ILs have been confirmed by observing the Raman spectral peaks at around 598 cm^{-1} and 702 cm^{-1}, which are from non-planar conformer, and around 624 cm^{-1} which is from planar conformer.[33] All three peaks (598 cm^{-1}, 622 cm^{-1}, and 704 cm^{-1}) are present in $[Emim]^+[TCB]^-$ Raman spectrum.

Table 3: Vibrational assignments of experimental and computed IR and Raman spectra of $[Emim]^+[TCB]^-$.[a,b,c] The calculated spectra were corrected using scaling factor of 0.958 at B3LYP/6-31+G(d, p) level.

B3LPY/6-31+G(d,p)						Assignment[d]	Experimental Spectra	
conformer (a)			conformer (d)					
ν_{cal}	I_{ir}	I_{Raman}	ν_{cal}	I_{ir}	I_{Raman}		ν_{ir}	ν_{Raman}
410	0.004	0.005	432	0.006	0.018	ring-C op bend		
463	0.033	0.000	463	0.000	0.034	$B(CN)_4$ sym str		445(0.10)
468	0.002	0.039	468	0.039	0.003	anion BCN bend and str		
472	0.003	0.036	472	0.036	0.003	anion BCN bend and str		486(0.24)
500	0.008	0.032	500	0.031	0.008	anion BCN bend	494(0.24)	
514	0.014	0.003	514	0.004	0.015	anion BCN bend		
515	0.016	0.000	515	0.000	0.016	anion BCN bend		522(0.15)
569	0.027	0.054	571	0.019	0.029	ring op deformation, ring-C7 str		
602	0.002	0.109	600	0.029	0.002	ring op deformation		598(0.19)
630	0.004	0.247	608	0.305	0.005	ring op deformation	622(0.36)	622(0.05)
676	0.011	0.056	682	0.054	0.011	ring-C str, ring ip deformation	646(0.26)	650(0.10)
708	0.001	0.257	710	0.270	0.001	ring-H op bend	702(0.12)	704(0.11)
775	0.000	0.016	779	0.034	0.001	ethyl CH_2 and CH_3 rock	747(0.35)	753(0.09)
795	0.002	0.409	805	0.420	0.002	ring-H9 op bend		807(0.09)
823	0.006	0.011	824	0.009	0.005	ring HCCH op bend	839(0.34)	
878	0.006	0.524	878	0.525	0.007	anion CBC asym str		854(0.10)
889	0.007	0.572	889	0.578	0.008	anion CBC asym str		

Continued on next page

Table 3 – *Continued from previous page*

B3LYP/6-31+G(d,p)						Assignment[d]	Experimental Spectra	
conformer (a)			conformer (d)					
ν_{cal}	I_{ir}	I_{Raman}	ν_{cal}	I_{ir}	I_{Raman}		ν_{ir}	ν_{Raman}
925	0.049	0.048	935	0.020	0.017	C7-C8 str		
941	0.015	1.000	941	1.000	0.016	anion BC str	928(1.00)	
994	0.038	0.007	997	0.006	0.029	ring ip asym str		960(0.15)
1003	0.016	0.007	1006	0.007	0.025	ring ip asym str, C77-C8 str		
1058	0.037	0.040	1061	0.019	0.029	ethyl CH_3 bend		1026(0.22)
1065	0.006	0.014	1070	0.024	0.009	methyl bend		
1081	0.013	0.066	1083	0.071	0.015	ring HCCH sym bend		
1095	0.009	0.012	1112	0.035	0.009	ethyl HCH rock	1091(0.10)	1090(0.16)
1112	0.005	0.014	1121	0.019	0.002	methyl HCH rock	1109(0.09)	
1139	0.008	0.762	1135	0.704	0.011	ring CH ip bend	1167(0.56)	1169(0.11)
1221	0.014	0.002	1239	0.091	0.003	ring CH ip bend, ethyl HCH twist	1251(0.03)	1252(0.12)
1265	0.004	0.001	1271	0.013	0.028	ring CH ip bend, ethyl HCH twist		
1300	0.112	0.061	1286	0.045	0.063	ring ip sym str, ethyl HCH twist		
1340	0.005	0.076	1315	0.153	0.063	ethyl HCH wag	1338(0.09)	1339(0.21)
1363	0.035	0.025	1361	0.001	0.032	ring ip asym str, ethyl CH_3 wag		
1371	0.032	0.036	1369	0.080	0.051	ring ip asym str, ethyl CH_3 wag		
1392	0.096	0.013	1391	0.094	0.057	ring ip asym str, ethyl HCH twist	1391(0.07)	1392(0.21)
1401	0.069	0.050	1408	0.016	0.056	methyl wag		
1429	0.055	0.087	1436	0.139	0.051	methyl CH_3 HCH bend		1422(0.31)
1436	0.048	0.086	1440	0.028	0.080	ethyl CH_3 HCH bend	1430(0.09)	
1438	0.075	0.063	1446	0.103	0.068	ethyl CH_3 HCH bend		
1456	0.010	0.099	1452	0.040	0.013	ethyl HCH bend		1452(0.20)
1458	0.064	0.113	1454	0.105	0.074	methyl HCH bend	1457(0.13)	
1540	0.016	0.346	1546	0.378	0.018	ring ip asym str, ethyl HCH bend		
1548	0.018	0.282	1549	0.192	0.022	ring ip asym str, methyl HCH bend	1572(0.23)	1570(0.14)
2214	0.218	0.016	2214	0.016	0.230	anion CN str		
2219	0.123	0.010	2219	0.009	0.125	anion $(CN)_2$ asym str		
2221	0.607	0.007	2222	0.007	0.623	anion $(CN)_2$ sym str	2222(0.02)	2225(1.00)
2237	0.720	0.013	2237	0.013	0.746	anion CN str		
2923	0.836	0.127	2925	0.094	1.000	ethyl CH_3 sym str	2912(0.01)	
2943	1.000	0.217	2945	0.187	0.975	methyl CH_3 sym str		
2970	0.376	0.015	2943	0.183	0.728	ethyl CH_2 sym str		2967(0.43)
2990	0.343	0.123	2987	0.092	0.461	ethyl CH_2 and CH_3 asym str	2989(0.04)	
3001	0.533	0.106	3003	0.033	0.352	ethyl CH_2 and CH_3 asym str		
3025	0.068	0.010	3009	0.064	0.197	ethyl CH_2 and CH_3 asym str		
3028	0.297	0.037	3030	0.011	0.302	methyl CH_3 HCH asym str		

Continued on next page

Table 3 – *Continued from previous page*

B3LPY/6-31+G(d,p)						Assignment[d]	Experimental Spectra	
conformer (a)			conformer (d)					
ν_{cal}	I_{ir}	I_{Raman}	ν_{cal}	I_{ir}	I_{Raman}		ν_{ir}	ν_{Raman}
3043	0.245	0.039	3050	0.011	0.164	methyl CH_3 HCH asym str		
3162	0.100	0.286	3163	0.088	0.225	ring C_2-H_9 str	3118(0.09)	3113(0.15)
3164	0.203	0.092	3176	0.333	0.023	ring HCCH asym str	3157(0.10)	
3181	0.468	0.049	3181	0.009	0.595	ring HCCH sym str, CH str		3175(0.20)

[a]The spectra were assigned by visualizing displacements of atoms around their equilibrium positions and via PED (potential energy distribution) analysis (see supporting information for PED data). [b] Wavenumbers in unit of cm^{-1}. [c] Both experimental and calculated intensities are normalized by their respective most intense bands. [d]ip: in plane; op: out of plane.

Conclusion

In summary, Density Functional Theory predicted four stable ion pair conformers for the Ionic liquid $[Emim]^+[TCB]^-$, in which, the $[Emim]^+$ cation adopts a non-planer structure in the most stable conformation. Atoms-in-molecules (AIM) analysis indicated the existence of several inter-ionic hydrogen bonds in the ion pair. Interaction energy calculations indicate that $[Emim]^+[TCB]^-$ has weaker inter-ionic interactions compared to the $[Emim]^+[BF_4]^-$ ion pair. Further, Natural Energy Decomposition Analysis (NEDA) calculations conclude that the decrease in the interaction energy is mainly due to the electrical component, which include both the electrostatic (ES) and polarization (POL) contributions. Assignments of the experimental and computed IR and Raman spectra were done by visualizing atoms around their equilibrium positions and through Potential Energy Distribution (PED) analysis. A red shift observed for $[Emim]^+[TCB]^-$ relative to $[Emim]^+[BF_4]^-$ also indicates a decrease in inter-ionic interaction in $[Emim]^+[TCB]^-$ ionic liquids.

References

(1) Vygodskii, Y. S.; Sapozhnikov, D. A.; Shaplov, A. S.; Lozinskaya, E. I.; Ignat'Ev, N. V.; Schulte, M.; Vlasov, P. S.; Malyshkina, I. A. *Polymer Journal* **2011**, *43*, 126–135.

(2) Kuang, D.; Wang, P.; Ito, S.; Zakeeruddin, S. M.; Grätzel, M. *Journal of the American Chemical Society* **2006**, *128*, 7732–7733.

(3) Zhou, D.; Bai, Y.; Zhang, J.; Cai, N.; Su, M.; Wang, Y.; Zhang, M.; Wang, P. *Journal of Physical Chemistry C* **2011**, *115*, 816–822.

(4) Scheers, J.; Johansson, P.; Jacobsson, P. *Journal of the Electrochemical Society* **2008**, *155*, A628–A634.

(5) Domanska, U.; Marciniak, A. *Journal of Physical Chemistry B* **2010**, *114*, 16542–16547.

(6) Yan, P.-F.; Yang, M.; Liu, X.-M.; Wang, C.; Tan, Z.-C.; Welz-Biermann, U. *Journal of Chemical Thermodynamics* **2010**, *42*, 817–822.

(7) Domańska, U.; Królikowska, M.; Jr.c, W. E. A.; Baker, G. A. *Journal of Chemical Thermodynamics* **2011**, *43*, 1050–1057.

(8) Mahurin, S. M.; Lee, J. S.; Baker, G. A.; Luo, H.; Dai, S. *Journal of Membrane Science* **2010**, *353*, 177–183.

(9) Linert, W.; Camard, A.; Armand, M.; Michot, C. *Coor* **2002**, *226*, 137–141.

(10) Babarao, R.; Dai, S.; en Jiang, D. *Journal of Physical Chemistry B* **2011**, *115*, 9789–9794.

(11) Becke, A. D. *Journal of Chemical Physics* **1993**, *98*, 5648–5652.

(12) Lee, C.; Yang, W.; Parr, R. G. *Physical Review B: Condensed Matter and Materials Physics* **1988**, *37*, 785–789.

(13) Frisch, M. J. et al. Gaussian 09. Revision A.1; Gaussian Inc. Wallingford CT 2009.

(14) Frisch, M. J.; Pople, J. A.; Binkley, J. S. *Journal of Chemical Physics* **1984**, *80*, 3265–3269.

(15) Jansen, H. B.; Ros, P. *Chemical Physics Letters* **1969**, *3*, 140–143.

(16) Boys, S. F.; Bernardi, F. *Mol. Phys.* **1970**, *19*, 553–566.

(17) Szczesniak, M. M.; Scheiner, S. *J. Chem. Phys.* **1986**, *84*, 6328–6335.

(18) Glendening, E. D.; Streitwieser, A. *Journal of Chemical Physics* **1994**, *100*, 2900–2909.

(19) Koch, U.; Popelier, P. L. A. *Journal of Physical Chemistry* **1995**, *99*, 9747–9754.

(20) Popelier, P. L. A. *Journal of Physical Chemistry A* **1998**, *102*, 1873–1878.

(21) Granovsky, A. A. Firefly. Version 7.1.G; www http://classic.chem.msu.su/gran/firefly/index.html.

(22) Turner, E. A.; Pye, C. C.; Singer, R. D. *Journal of Physical Chemistry A* **2003**, *107*, 2277–2288.

(23) Umebayashi, Y.; Fujimori, T.; Sukizaki, T.; Asada, M.; Fujii, K.; Kanzaki, R.; ichi Ishiguro, S. *Journal of Physical Chemistry A* **2005**, *109*, 8976–8982.

(24) Tsuzuki, S.; Tokuda, H.; Hayamizu, K.; Watanabe, M. *Journal of Physical Chemistry B* **2005**, *109*, 16474–16481.

(25) Bader, R. F. W. *Chemical Reviews* **1991**, *91*, 893–928.

(26) Schenter, G. K.; Glendening, E. D. *Journal of Physical Chemistry* **1996**, *100*, 17152–17156.

(27) Glendening, E. D. *Journal of the American Chemical Society* **1996**, *118*, 2473–2482.

(28) Reed, A. E.; Curtiss, L. A.; Weinhold, F. *Chemical Reviews* **1988**, *88*, 899–926.

(29) WEINHOLD, F.; LANDIS, C. R. *Chemistry Education Reearch and Practice in Europe* **2001**, *2*, 91–104, Done.

(30) Küppers, T.; Bernhardt, E.; Willner, H.; Rohm, H. W.; Köckerling, M. *Inorganic Chemistry* **2005**, *44*, 1015–1022.

(31) Buffeteau, T.; Grondin, J.; Lassègues, J.-C. *Applied Spectroscopy* **2010**, *64*, 112–119.

(32) Grondin, J.; Lasségues, J.-C.; Cavagnat, D.; Buffeteau, T.; Johansson, P.; Holomb, R. *Journal of Raman Spectroscopy* **2011**, *42*, 733–743.

(33) Heimer, N. E.; Sesto, R. E. D.; Meng, Z.; Wilkes, J. S.; Carper, W. R. *Journal of Molecular Liquids* **2006**, *124*, 84–95.

Graphical TOC Entry